Melting, melting competition, and structural transitions between shell-closed icosahedral and octahedral nickel nanoclusters

Zhi Zhang,[1,2] Wangyu Hu,[1,*] and Shifang Xiao[1]
[1]*Department of Applied Physics, Hunan University, 410082 Changsha, Hunan, People's Republic of China*
[2]*Department of Physics and Chemistry, Henan Polytechnic University, 454000 Jiaozuo, Henan, People's Republic of China*
(Received 9 July 2005; revised manuscript received 17 February 2006; published 30 March 2006)

The surface premelting, melting behavior, melting competition, and structural transition of shell-closed icosahedral (ICO) and cuboctahedral (CUB) nickel clusters with atoms from 309 to 2057 were discussed extensively by using quantitative caloric curves based on the modified analytic embedded atom method and molecular dynamics, qualitative three-dimensional structural visualization of symmetric truncation, and the radial number distribution function. These studies reveal that smaller clusters melt at lower temperatures and a solid-to-solid structural transition occurs from CUB to ICO structure during melting process. The shell-closed ICO clusters could only be preferred until 923 atoms at temperatures no higher than 1380 K, which is in agreement with the experiments. The melting temperature of larger clusters would depend on their starting structures, which can be attributed to surface premelting.

DOI: 10.1103/PhysRevB.73.125443 PACS number(s): 61.44.Br, 61.46.−w, 64.70.Dv, 64.70.Nd

I. INTRODUCTION

Melting of clusters is one of the hot spots in materials science. Recently published theoretical considerations,[1–4] computational simulations,[5–27] and experimental observations[28–41] support the conclusion that the melting temperature depends strongly on cluster size. In addition, structural transition in small clusters during the melting process was reported.[42–44] Ni clusters are ferromagnetically and superparamagnetically interesting and have substantial applications in the physics and chemistry of transition metals.[45–47]

Because of the limitation of computers, the melting behavior of small clusters with about 100 atoms is of primary computational interest, involving Ni,[5,6,9,13] Ag,[10,13] Au,[8,10,13] Cu,[10,13,22] Pd,[13] Pt,[13] Pb,[13], Al,[13] Si,[14] Na,[18–21] K/I ions,[17] etc. In thermodynamics of small Ni clusters published by Nayak *et al.*,[6] small clusters consisting of 7–23 atoms were studied by tight-binding many-body potential molecular dynamics (MD). The melting temperature was found to be a nonmonotonic function of cluster size. With the development of computer technology, cluster research has penetrated into the areas of large clusters. Wen and co-workers studied size effects on the melting of Ni nanowires by using a constant temperature and constant stress (NPT) MD with the modified quantum corrected Sutten-Chen many-body potential (QSC).[25] The melting temperatures for both Ni bulk and nanowire are lower than the experimental value of 1728 K for pure fcc Ni. Qi and his partners studied melting of Ni nanoclusters with up to 8007 atoms (5.7 nm) using QSC, but their cluster geometries were constructed by spherically truncating a large fcc Ni block, and the extrapolation of the melting temperatures for the spherical fcc clusters is significantly below the calculated value of 1760 K for bulk Ni too.[15] Our inerest is in the available melting temperature for larger icosahedral Ni clusters and how large such clusters can be within what temperature range.

Geometrical shell closings show the importance of the melting process.[19,21,26] There are a variety of structures which may be postulated for geometric shell metal clusters, such as the cuboctahedron (CUB), a fragment of the fcc lattice; the icosahedron (ICO); the truncated decahedron (DEC); and the rhombic dodecahedron (RHO), a fragment of the bcc lattice.[3] ICO clusters with complete geometric shells resist meltage when heated and thus have higher thermal stability[28,29] or melting temperatures.[16,18,26] These clusters are formed either by shell-by-shell[48] growth over smaller and energetically favorable ICO cores, or by a solid-state transformation of small decahedra into larger ICO.[42–44,49] In a near-threshold photoionization experiment and standard time-of-flight mass spectrometry, Pellarin and his copartners found that Ni and Co clusters are of ICO atomic structure in the studied mass range (50–800 atoms).[29] Martin experimentally proved the ICO stability by using a second laser to evaporate Na clusters and detecting such clusters as magic numbers within mass spectra.[29,30] Nayak *et al.*[6] and Lee *et al.*[9] simultaneously found that Ni_{13}, the smallest close-packed ICO Ni cluster, has the highest melting temperature in the size range studied. Thus, for small clusters, both experiments and simulations tend to stabilize ICO symmetries. As is well known, bulk Ni prefers fcc structure and CUB clusters are constructed by truncating an octahedron by a cube which has the stacking sequence characteristic of a fcc lattice.[29] Therefore, for large Ni clusters, the thermodynamic behavior of CUB clusters ought to be similar to fcc bulk. The great advantage of CUB clusters is that its total surface area is small and the total number of atoms is the same as in ICO clusters of the same shells.[29] Obviously, structural and melting competitions between ICO and CUB Ni clusters are inevitable. The critical size was predicted to be 1415 atoms.[50] In the literature[53] without mentioning temperature, the closed-shell perfect ICO Ni clusters were discussed to remain stable up to a size $N=250\,000$. Our wonder is the transition from ICO to CUB and competition between ICO and CUB upon heating.

Reported by Rey *et al.*[5] on molecular-dynamics study of the binding energy and melting of transition-metal Ni_N, Pd_N,

Au_N, and Ag_N clusters ($N=2-23$), the applicability of the embedded atom model (EAM) is questionable for systems with few particles. Whether EAM is available for melting of large clusters will be a challenge.

The recent work by Jarrold on melting, premelting, and structural transitions in size-selected Al clusters with around 55 atoms clearly demonstrated that the thermodynamic melting temperature cannot depend on the isomers employed to start the heating runs.[38] But we are curious about the dependence of melting points on starting structural configurations of clusters because of different melting mechanisms for different size ranges.[51]

To reply to the above questions, we utilized the analytical character of the modified analytic embedded atom method (MAEAM)[52,55] to study the melting behavior and competition of relatively large ICO and CUB Ni clusters of hundreds to thousands of atoms. The size range we are interested in is based on one of the three distinctive melting mechanisms, the surface premelting model (SPM), as for size-selected isolated silver nanoparticles with 258 to 3871 atoms[54]and the preference of geometric shell closing to electronic shell closing during melting process for Na clusters with 147 atoms[21] or more.[29]

The present work has focused on the melting competition of closed-shell ICO and CUB Ni clusters of size from 309 to 1415 atoms. Surface premelting, melting and melting competition, and structural transition during melting are investigated. ICO clusters are preferable to CUB clusters until the critical size near 923 atoms takes place at about 1380 K, which is consistent with the experimental observation for Ni clusters.[28] However, ICO and CUB clusters over 561 atoms have their own melting temperatures without structural transformations, which is inconsistent with the experimental evidence for Al clusters.[38] The last section presents a brief summary of our study.

II. COMPUTATIONAL SCHEME

In this paper, the internal energy of a cluster has to be evaluated with respect to temperature. Potential energy is based on the MAEAM scheme in which the total interaction or binding energy of an N-atom system is made up of three parts: an embedding energy function[51] determined by the superposition of electronic densities of effective atoms except the embedded one, a pairwise interaction potential due to a core-core repulsion,[52] and a modification term[56–60] to correct the assumption of the linear superposition and spherical symmetry of electronic densities in the original EAM.[51] In the above scheme, all parameters in application to the coming ICO and octahedral environment are ascertained by fitting the geometrical and physical attributes such as the nearest neighbors, the cohesive energy, the vacancy formation energy, the elastic constants, the lattice constants, and the equilibrium state. All the parametrized quantities for fcc-like Ni atoms are tabulated in Ref. 52. This model has been employed to theoretically reproduce the structures and stabilities for Ni clusters,[53] which are consistent with experimental evidences.[28]

In order to determine the structural information of concentric shell clusters when the temperature changes, the radial number distribution (RND) of atoms was introduced to denote the ratio of atoms within spherical shells to the total of the cluster. The center of all these concentric spherical shells is located at the mass center of the cluster. The radial asymmetry of atoms, especially those in the surface of a cluster, causes the preferable dislocation of the atoms in the radial direction. Therefore, this kind of function is sufficient to monitor the structural evolution of clusters with temperature elevation.

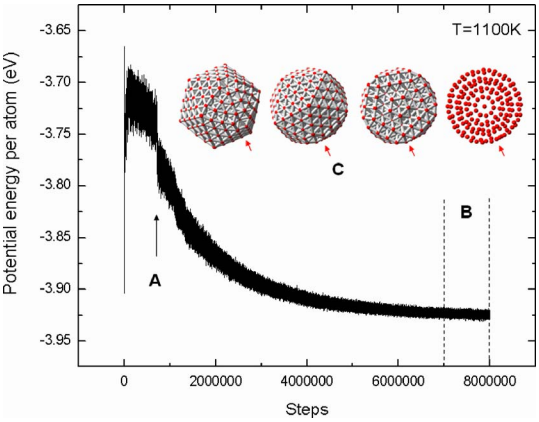

FIG. 1. (Color online) Potential energy per atom with respect to equilibration time steps for CUB 309-atom cluster at 1100 K. Label A shows the structural transition from CUB to ICO cluster, label B is the time range for reliable statistics, and label C stands for the surface deformation of transmitted ICO cluster. All four 3D pictures exhibit the same averaged configurations, from left to right, respectively, in the perspective, the top view, the truncated top view, and the top view without bonds.

First of all, the atomic sites of clusters studied in this paper are geometrically generated according to Mackay[61] multishell ICO and CUB configurations[29] and radially optimized by energetic consideration.[51] The energy optimizations due to the MAEAM are performed shell by shell, maintaining the core rigid to determine the cluster size until the minimum binding energy with no consideration of temperature. Within the NVT[55]-without-PBC (periodic boundary conditions) MD equilibration of the MAEAM potentials at given temperatures from concerned temperature to over the experimental value 1728 K of the melting point of bulk fcc Ni with the fewest steps of 10 K, each cluster is heated from its initially energy-optimized configuration and equilibrates at each temperature for 8 ns to attain the last 1 ns average of the total energies and site coordinates for probing the melting point and competition of ICO and CUB clusters. Figure 1 shows the equilibrating procedure of potential energy of the CUB 309-atom cluster at 1100 K as an instance of reliable and sufficient equilibration, and the plot is for the potential energy per atom as the function of time steps of 1.0 fs. The equations of motion are integrated with a four value gear algorithm (predictor-corrector) with the above time step and the linear and angular momenta are corrected at each temperature. Then, the melting behavior of close-packed ICO and CUB clusters was probed by the caloric curve, 3D visualization, and the RND function. Premelting occurs among surface atoms and melting temperature corresponds to thor-

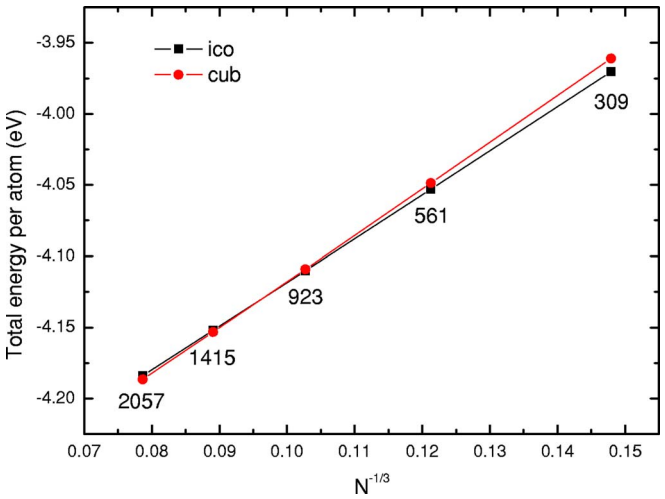

FIG. 2. (Color online) Radial optimization of ICO and CUB shell-closed nickel clusters by minimizing their energy. From the energetic point of view, ICO clusters are more stable than CUB clusters when the clusters are small at 0 K. The crossover occurs between 923- and 1415-atom clusters.

ough destruction of geometric structure from external surface into internal core.

III. RESULTS AND DISCUSSION

A. Cluster preparation

Structural preparation of distinct cluster configurations is the prelude of investigation into melting behavior of clusters. Clusters with well-defined geometry can be formed by packing shells of atoms on top of each other.[29] In this paper, geometrically predetermined cluster configurations, icosahedron and cuboctahedron, are shell-by-shell optimized by minimizing their binding energy with the radius of each concentric shell being optimized independently.[3] Such radial optimization of geometric shell clusters conserves the point group of the ICO and CUB clusters. Energetic determination of shell-closed ICO and CUB Ni configurations under 0 K is indicated in Fig. 2. For the same number of atoms in corresponding clusters of both ICO and CUB structures, small ICO clusters have lower energy than CUB clusters, which prefigures the preferable stability of ICO to CUB as compared with Fe clusters.[4] As clusters becoming larger and larger beyond the crossover in Fig. 2, CUB clusters tend to be more stable than ICO clusters because of their higher melting temperature.

B. Surface premeltage

During temperature elevation before clusters melted, surface premelting was reported on shell-unclosed Ni clusters[9] and shell-closed Au,[16], Na,[19,26], Cu,[27] and Ag (Ref. 54) clusters. For relatively larger clusters, they have a higher proportion of surface atoms, which are more weakly bound and less constrained in their thermal motion[62] than those in solid core. As to shell-closed Ni clusters, melting behavior starts in the outermost shell and atoms on vertices are pioneers to dislocate their position because of the structural asymmetry as a result of the fact that the average coordination number of the surface atoms is less than that of the bulk atoms for clusters of certain sizes as stated in Ref. 23. When mobile outer atoms lost their original locations, surface premelting comes into stage and both solidlike and liquidlike structures coexist as an indication of a finite-size effect.[31] From an energetic point of view, the absence of the sharp change in the slope and the nearly linear increase of total energy of a cluster are insufficient to be used to identify the premelting as indicated in Figs. 3 and 4. However, structural visualization will assist in the identification as shown in the inset figures. Because there is no sign to recognize at which temperature the premelting begins, it is exhausting work to determine the premelting temperature. Fortunately, a shell-periodic cluster has one central atom and all other atoms are concentrically distributed around the central one. So the RND is introduced to

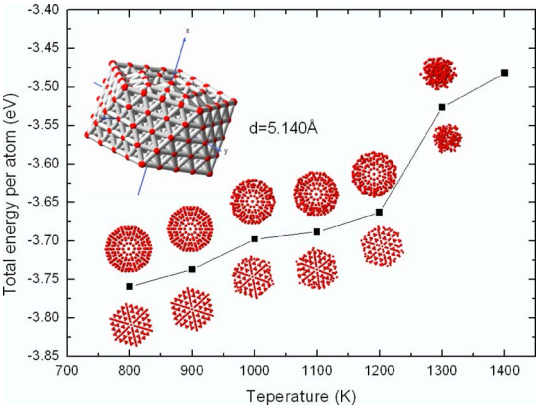

FIG. 3. (Color online) Total energy per atom as a function of cluster temperature and symmetrically truncated visualizations for ICO Ni clusters with 309 atoms. The thickness of the truncated clusters is $d=5.14$ Å. Corresponding to each temperature as temperature increases before totally melting, surface premeltage is clearly visualized. The upper visualizations are symmetrically truncated by parallel planes with the z (fivefold) axis as their normal direction and the lower visualizations are symmetrically truncated by parallel planes with the x (threefold) axis as their direction. The bonds among atoms are only to guide the eye and the coordinate frames are for special reference.

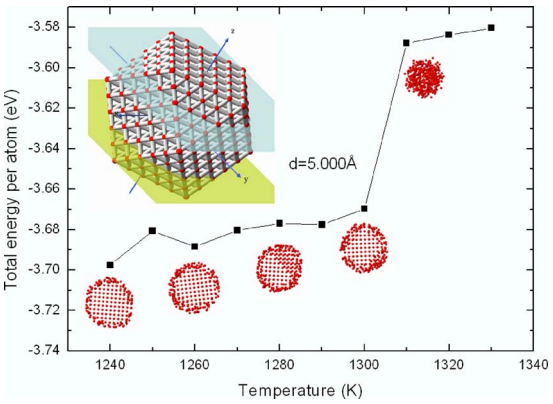

FIG. 4. (Color online) The analogy to Fig. 2 but for CUB Ni clusters with 561 atoms and only one-directional visualizations.

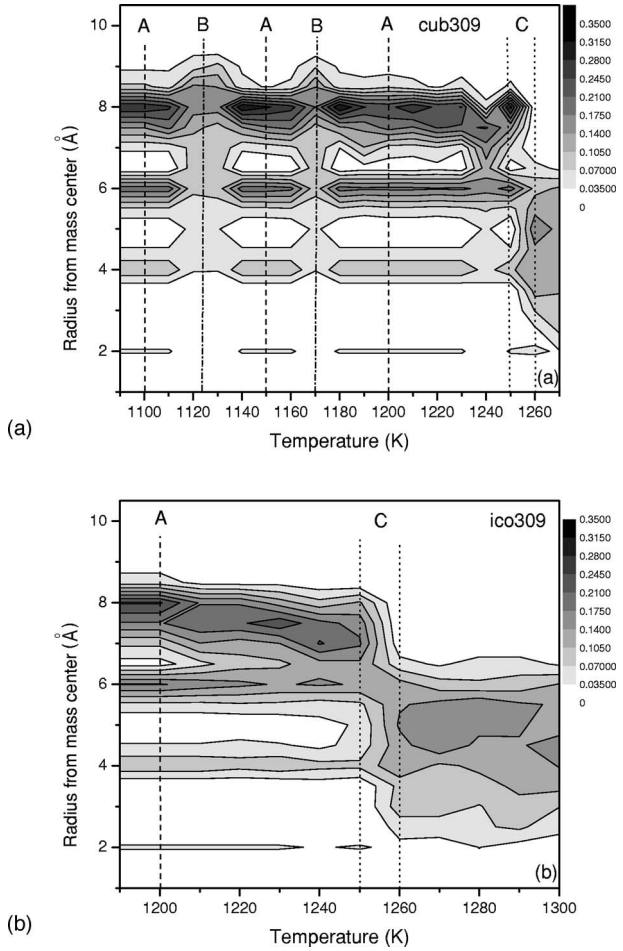

FIG. 5. Contour plot of radial number distribution against temperature. Subplot (a) stands for CUB Ni_{309} and (b) for ICO Ni_{309}. Gray-scale legends represent the relative number of atoms along radial direction from mass center of clusters. Label A (dash lines) stands for ICO character, label B (dash-dot lines) for CUB, and label C (dot lines) for the melting range. At the lower temperature range, clusters remain in their geometric structures, which are of parallel horizontal lines in the plots. As temperature rises, atoms in the outer shells start to displace and surface premelting occurs or the contour lines with larger radius are no longer parallel. To melting temperature, structural destruction in the core with small radius occurs at which all parallel lines disappear. In subplot (a), some of the contour structure between premelting and melting shows the identity compared with the ICO structure at the lower temperature range in subplot (b), which poses the implication of structural transition between CUB and ICO clusters.

demonstrate such concentric symmetry as shown in Figs. 5 and 6, in which radial distance from the mass center of a cluster and the cluster temperature are variables, and the gray-scale-filled contour, as a function, shows the relative number of atoms in a spherical shell of radius r and thickness $\Delta r = 0.05$ nm. Before premelting of a cluster, all atoms undergo thermal vibrations about their corresponding equilibrium positions and the cluster geometry remain unchanged. As temperature elevates, atoms in the outermost shell of a cluster vibrate more and more violently and the asymmetric interaction between surface and inner atoms leads to prior dislocation of these atoms. The dislocation occurs on the vertices and then edges and then faces, which is analogous to Na clusters.[19,26] The structural distortion of the primary symmetry means the prelude of premelting. From surface to core, premelting develops deeper and deeper toward the inner core until the whole structural symmetry is destroyed. At this temperature, melting point is reached. The size range in our simulations from 309 to 1415 atoms is consistent with that in the literature,[54] which can be well explained by the surface premelting models.

C. Melting and structural transitions

Structural transitions for small clusters were found in many literatures.[42–44] Pair correlation function (PCF),[18] common neighbor analysis (CNA),[8] radial distribution function (RDF),[52] and root-mean-square bond length (RMS)[22] are usually used to evaluate these deformations, which are indirect ways to detect structural transitions and have some shortcomings for surface and core disordering. In the present work, RND is employed instead of PCF, CAN, RDF, and RMS.

Figure 7 shows the temperature dependence of the total energy per atom and cluster visualization. Taking the caloric curve (dot lines) of ICO clusters as a reference, we plot the total energy per atom for CUB clusters along with some symmetrically truncated structural visualization at certain typical temperature. During the melting process of CUB Ni clusters with 309 atoms, CUB-to-ICO structural transitions within the solid phase take place near 1100, 1150, and 1200 K as indicated in Fig. 5, in which each type of cluster is characterized by its RND patterns. Near 1122 and 1170 K, RND patterns are CUB characterized. Therefore, the distinct RND patterns between ICO and CUB clusters are well resolved. Such CUB-ICO structural transitions are clearly distinguishable in Fig. 7, where the total energy per atom for the CUB cluster of 309 atoms drops to near that for the ICO cluster. As the clusters grow larger, such transitions vanish as exemplified in Fig. 6 for the clusters with 561 and 923 atoms. The reason for the CUB-ICO transition and the disappearance of that transition is not clear upon the present work and needs further exploration.

D. Melting and melting competition

The variation of the average total energy per atom of shell-closed clusters consisting of 309, 561, 923, 1415, and 2057 atoms as a function of temperature reflects caloric curves of these clusters, as plotted in Fig. 8(a) for CUB structure and Fig. 8(b) for ICO structure. The average total energy per atom increases monotonically with temperature for these relatively large clusters with closed atomic shells with the exception of mild fluctuation, which is analogous to the smallest Ni cluster with 13 atoms.[6,9] The steeper ascent of the caloric curves corresponds to the overall melting of the clusters. The solid-to-liquid melting process occurs over a broad range of temperature-surface premelting. As for our 10 K interval simulations, the melting temperatures for clusters of different sizes and different structures can be approximately determined within the 10 K range as listed in Table I.

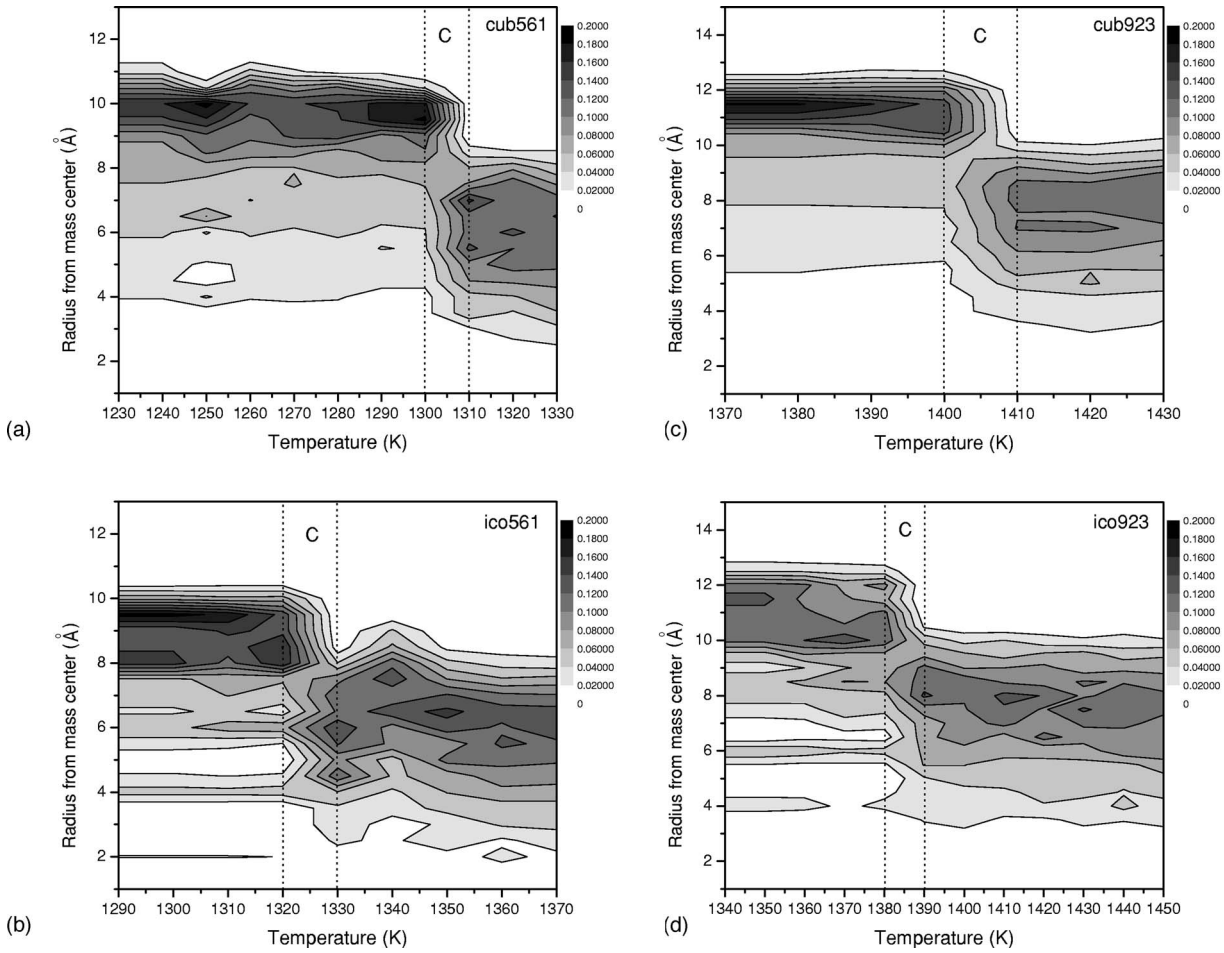

FIG. 6. The analogy to Fig. 5 but (a) for CUB Ni_{561}, (b) for ICO Ni_{561}, (c) for CUB Ni_{923}, and (d) for ICO Ni_{923}. As clusters grow larger, the structural transition no longer exists.

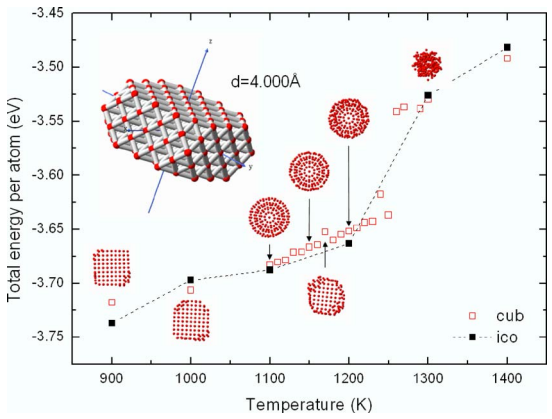

FIG. 7. (Color online) Total energy per atom as a function of cluster temperature and symmetrically truncated structural visualizations of melting evolution of four-shell CUB clusters with 309 atoms. The thickness of the truncated clusters is d=4.000 Å. The dot line as a reference is for ICO cluster with 309 atoms as plotted in Fig. 3. Below 1000 K, the clusters maintain their starting CUB configuration. Through 1000 K below the melting point, CUB clusters are likely to take ICO configuration.

The melting temperature drops dramatically with smaller and smaller clusters in the nanoscale region, resulting in the melting temperature of a 309-atom ICO Ni cluster 27.3% lower than of Ni bulk. The present result is more satisfactory than what was released by Qi[15] and co-workers in which clusters are constructed by spherically truncating a large fcc Ni block. The reason for this is that shell-completed ICO clusters are more closely packed, of relatively fewer surface atoms and consequently more stable than the spherical cutoff geometries out of a large fcc Ni block.

For the shell-closed Ni clusters studied, the theoretical evidence of consistently higher melting point of ICO structure than that of CUB structure reminds one that the ICO configuration is more thermally stable than the CUB one. One may also wonder to what size and to what extent the clusters remain the ICO structure because fcc structure is the terminal for Ni bulk, while the structure between ICO shells is hcp.[30] To answer this question, the melting temperatures and their corresponding linear-fitted extrapolation to bulk are plotted against cluster size as shown in Fig. 9 for both ICO and CUB clusters, which is similar to that in Ref. 3 for Fe clusters. The two fitted lines cross at approximately 1380 K and about 923 atoms. It can be concluded that ICO Ni clusters larger than between shell-closed clusters with 561 and 923 atoms[29] are less stable than CUB clusters which are

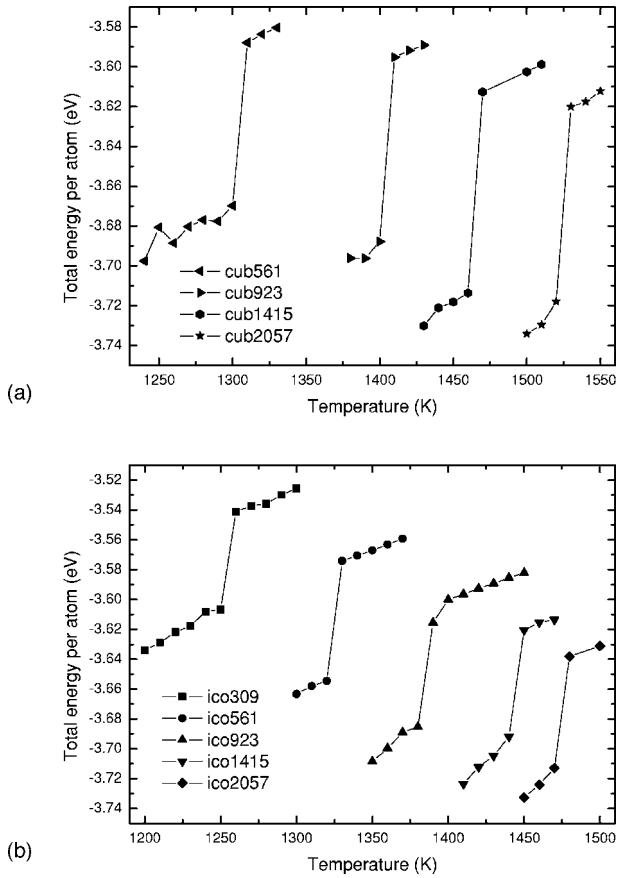

FIG. 8. Dependence of total energy per atom and cluster size with different atoms on temperature. (a) Stands for shell-closed CUB Ni clusters and (b) for ICO ones. These plots are analogous to caloric curves of corresponding clusters. The sharp increases of the curves indicate that cluster melting takes place in the 10 K range, as in our computations.

truncated from fcc bulk. This result would be of a certain value to practical applications and in agreement with the experimental observation[28] where no temperature was mentioned and the magic numbers in mass spectra of clusters with more than 561 atoms were not clearly characterized by ICO configurations.

The extrapolated melting temperatures of CUB and ICO clusters from linear fit lines of the overall melting temperatures to the bulk are 1923 and 1726 K, respectively. Our calculated value of the melting temperature for Ni bulk is 1731 K, which is near 1726 K but significantly far from

TABLE I. Melting range of shell-closed Ni clusters (K).

Atoms	CUB	ICO
309		1250–1260
561	1300–1310	1320–1330
923	1400–1410	1380–1390
1415	1460–1470	1440–1450
2057	1520–1530	1470–1480
to bulk	1923	1726

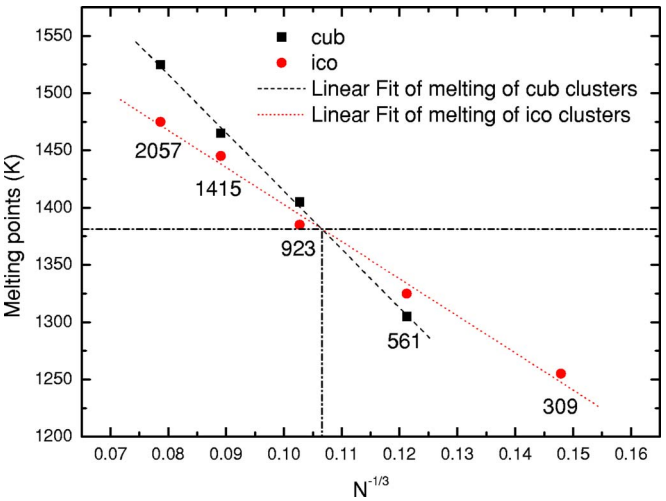

FIG. 9. (Color online) Plot of melting temperatures of shell-closed Ni clusters against the inverse cluster size and their linear fit lines for both CUB (dash line) and ICO (dot line) clusters, respectively. Owning to structural transition, CUB Ni_{309} has no melting point. For clusters larger than 309 atoms, the melting points do exist for both CUB and ICO clusters without structural transitions. As clusters of higher melting temperature are thermodynamically preferable, small clusters of fewer 923 atoms prefer ICO configuration while larger clusters of more than 923 atoms prefer CUB configuration, a fcc fragmentation. The crossover is near the 923-atom cluster at about 1380 K. The dash-dot lines are only a guide for the eye.

1923 K. Although the reason for the difference is not clear as mentioned in Ref. 25 for Ni nanowires, a little decrease of melting temperature for Ag_{3871} from the linear fit[51] may be an implication to be used to explain the possible existence of nonlinear extrapolation when clusters become so large.

Jarrold and his research group recently reported in their experimental mass spectra[38] for size-selected Al clusters with around 55 atoms that the thermodynamic melting point cannot depend on the isomers employed to start the heating runs and there can only be one melting temperature because all isomers should convert into the lowest energy form as the melting temperature is approached. In our opinion, structural transitions are popular for small clusters but surface premelting is more preferable for large clusters. Overall melting of a cluster immediately follows complete surface premelting. While surface premelting prevails, the inner core keeps its original structure as simulated in this work. Below melting temperature, therefore, the existence of CUB or ICO clusters would be dependent on their starting configurations, and the melting competition between CUB and ICO Ni clusters would occur near the size of 923 atoms. Higher melting temperature for smaller Na clusters as reported by Aguado *et al.*[20,21] and Itoh *et al.*[19] has no demonstration for Ni clusters of the size range of interest.

IV. SUMMARY

Through the analysis of the melting process by MAEAM within MD for CUB and ICO Ni clusters, ICO clusters keep

higher thermal stability than CUB clusters until the cluster size reaches as large as 923 atoms and the melting temperature is beyond 1380 K. The critical implication suggests that ICO clusters could exist at a size of about 3.2 nm in diameter, and CUB clusters, truncated out of fcc bulk, would be the last candidate for bulk Ni. For small clusters with 309 atoms or fewer, CUB-to-ICO structural transition appears in the melting process prior to solid-to-liquid phase transition because of the higher surface-to-volume atomic ratio 52.4% of both and the more closely packed geometric configuration of ICO clusters. With no exception for larger clusters, the melting evolution undergoes a surface premelting stage and an overall melting stage before the transformation to liquid phase, and the melting points are significantly lower than that of bulk Ni.

Suffice it to say that the present report on Ni clusters would be of both theoretical and applicable importance. Moreover, the MAEAM model is valid for all sizes of clusters with the exception of its uncertainty for small clusters with about tens of atoms. However, further work is expected to make clear the present report.

ACKNOWLEDGMENTS

This work has been financially supported by the National Science Foundation of China (NSFC, Grant No. 50371026) and the High Performance Computing Center of Hunan University.

*Email address: wangyuhu2001cn@yahoo.com.cn

[1] R. S. Berry and T. L. Beck, Adv. Chem. Phys. **70**, 75 (1988).
[2] S. K. Nayak, R. Ramaswamy, and C. Chakravarty, Phys. Rev. Lett. **74**, 4181 (1995).
[3] H. Cox, R. L. Jhonston, and J. N. Murrel, J. Solid State Chem. **145**, 517 (1999).
[4] K. K. Nanda, S. N. Sahu, and S. N. Behera, Phys. Rev. A **66**, 013208 (2002).
[5] C. Rey, L. J. Gallego, J. Garcia-Rodeja, J. A. Alonso, and M. P. Iniguez, Phys. Rev. B **48**, 8253 (1993).
[6] S. K. Nayak, S. N. Khanna, B. K. Rao, and P. Jena, J. Phys.: Condens. Matter **10**, 10853 (1998).
[7] C. L. Cleveland, W. D. Luedtke, and Uzi Landman, Phys. Rev. Lett. **81**, 2036 (1998).
[8] C. L. Cleveland, W. D. Luedtke, and Uzi Landman, Phys. Rev. B **60**, 5065 (1999).
[9] Y. J. Lee, J. Y. Maeng, E. Lee, B. Kim, S. Kim, and K. Han, J. Comput. Chem. **21**, 380 (2000).
[10] T. X. Li, Y. L. Ji, S. W. Yu, and G. H. Wang, Solid State Commun. **116**, 547 (2000).
[11] B. Güneş and Ş. Erkoç, Int. J. Mod. Phys. C **11**, 1567 (2000).
[12] V. E. Dmitrienko, S. B. Astaf'ev, and M. Kléman, Mater. Sci. Eng., A **294**, 413 (2000).
[13] Y. J. Lee, R. M. Nieminen, E. Lee, and S. Kim, Comput. Phys. Commun. **142**, 201 (2001).
[14] J. Wang, G. Wang, F. Ding, H. Lee, W. Shen, and J. Zhao, Chem. Phys. Lett. **341**, 529 (2001).
[15] Y. Qi, T. Çağin, W. L. Johnson, and W. A. Goddard III, J. Chem. Phys. **115**, 385 (2001).
[16] H. B. Liu, J. A. Ascencio, M. Perez, and M. J. Yacaman, Surf. Sci. **491**, 88 (2001).
[17] X. Zhu, X. You, R. Xiong, and Z. Zhou, Chem. Phys. **269**, 243 (2001).
[18] H. B. Liu, R. Perez, G. Ganizal, and J. A. Ascencio, Surf. Sci. **518**, 14 (2002).
[19] M. Itoh, V. Kumar, and Y. Kawazoe, Phys. Rev. B **73**, 035425 (2006).
[20] A. Aguado and J. M. López, Phys. Rev. Lett. **94**, 233401 (2005).
[21] A. Aguado, J. Phys. Chem. B **109**, 13043 (2005).
[22] S. Özçelik and Z. B. Güvenç, Surf. Sci. **532**, 312 (2003).
[23] L. Wang, Y. Zhang, X. Bian, and Y. Chen, Phys. Lett. A **310**, 197 (2003).
[24] Y. Wang, S. Teitel, and C. Dellago, Chem. Phys. Lett. **394**, 257 (2004).
[25] Y. Wen, Z. Zhu, R. Zhu, and G. Shao, Physica E (Amsterdam) **25**, 47 (2004).
[26] H. Haberland, Th. Hippler, J. Donges, O. Kostko, M. Schmidt, and B. von Issendorff, Phys. Rev. Lett. **94**, 035701 (2005).
[27] Y. Wang, S. Teitel, and C. Dellago, J. Chem. Phys. **122**, 214722 (2005).
[28] M. Pellarin, B. Baguenard, J. L. Bialle, J. Lermé, M. Broyer, J. Miller, and A. Perez, Chem. Phys. Lett. **217**, 349 (1994).
[29] T. P. Martin, Phys. Rep. **273**, 199 (1996).
[30] T. P. Martin, Solid State Ionics **131**, 3 (2000).
[31] H. W. Sheng, Z. Q. Hu, and K. Lu, Nanostruct. Mater. **9**, 661 (1997).
[32] M. Schmidt, R. Kusche, W. Kronmüller, B. von Issendorff, and H. Haberland, Phys. Rev. Lett. **79**, 99 (1997).
[33] M. Schmidt, R. Kusche, B. von Issendorff, and H. Haberland, Nature (London) **393**, 238 (1998).
[34] K. F. Peters, J. B. Cohen, and Y. W. Chung, Phys. Rev. B **57**, 13430 (1998).
[35] R. Kusche, Th. Hippler, M. Schmidt, and B. von Issendorff, Eur. Phys. J. D **9**, 1 (1999).
[36] D. Gerion, A. Hirt, I. M. L. Billas, A. Châtelain, and W. A. de Heer, Phys. Rev. B **62**, 7491 (2000).
[37] T. Bachels, H. J. Güntherodt, and R. Schafer, Phys. Rev. Lett. **85**, 1250 (2000).
[38] G. A. Breaux, C. M. Neal, B. Co, and M. F. Jarrold, Phys. Rev. Lett. **94**, 173401 (2005).
[39] M. Schmidt, R. Kusche, T. Hippler, J. Donges, W. Kronmuller, B. von Issendorff, and H. Haberland, Phys. Rev. Lett. **86**, 1191 (2001).
[40] G. Wrigge, M. A. Hoffmann, and B. von Issendorff, Phys. Rev. A **65**, 063201 (2002).
[41] M. Schmidt, J. Donges, Th. Hippler, and H. Haberland, Phys. Rev. Lett. **90**, 103401 (2003).
[42] M. W. Sung, R. Kawai, and J. H. Weare, Phys. Rev. Lett. **73**, 3552 (1994).
[43] A. Ghazali and J.-C. S. Lévy, Phys. Lett. A **228**, 291 (1997).

[44] T. X. Li, S. M. Lee, S. J. Han, and G. H. Wang, Phys. Lett. A **300**, 86 (2002).
[45] V. Bonacic-Koutechy, P. Fantucci, and J. Koutechy, Chem. Rev. (Washington, D.C.) **91**, 1035 (1991).
[46] I. M. L. Billas, J. A. Becher, A. Châtelain, and W. A. de Heer, Science **265**, 1682 (1994).
[47] S. E. Apsel, J. W. Emmert, J. Deng, and L. A. Bloomfield, Phys. Rev. Lett. **76**, 1441 (1996).
[48] F. Baletto, C. Mottet, and R. Ferrando, Phys. Rev. B **63**, 155408 (2001).
[49] F. Baletto, J. P. K. Doye, and R. Ferrando, Phys. Rev. Lett. **88**, 075503 (2002).
[50] J. M. Montejano-Carrizales, M. P. Iñiguez, and J. A. Alonso, J. Cluster Sci. **5**, 287 (1994).
[51] R. A. Johnson, Phys. Rev. B **41**, 9717 (1990).
[52] J. Yang, W. Hu, H. Deng, and D. Zhao, Surf. Sci. **572**, 439 (2004); B. Zhang, W. Hu, and X. Shu, *Theory of Embedded Atom Method and Its Applications to Materials Science—Atomic Scale Materials Design Theory* (Hunan University Press, Changsha, 2003).
[53] Z. Zhang, W. Hu, and S. Xiao, J. Chem. Phys. **122**, 214501 (2005); Z. Zhang and W. Hu, *Computational Physics—Proceedings of the Joint Conference of ICCP6 and CCP2003* (Rinton, Princeton, NJ, 2005), pp. 170–173.
[54] S. J. Zhao, S. Q. Wang, D. Y. Cheng, and H. Q. Ye, J. Phys. Chem. B **105**, 12875 (2001).
[55] W. Hu, S. Xiao, J. Yang, and Z. Zhang, Eur. Phys. J. B **45**, 547 (2005).
[56] W. Hu, H. Xu, X. Shu, X. Yuan, B. Gao, and B. Zhang, J. Phys. D **33**, 711 (2000).
[57] W. Hu, B. Zhang, B. Huang, F. Gao, and D. J. Bacon, J. Phys.: Condens. Matter **13**, 1193 (2001).
[58] W. Hu and M. Fukumoto, Modell. Simul. Mater. Sci. Eng. **10**, 707 (2002).
[59] W. Hu, X. Shu, and B. Zhang, Comput. Mater. Sci. **23**, 175 (2002).
[60] W. Hu, H. Deng, X. Yuan, and M. Fukumoto, Eur. Phys. J. B **34**, 429 (2003).
[61] A. L. Mackay, Acta Crystallogr. **15**, 916 (1962).
[62] R. R. Couchman, Philos. Mag. A **40**, 637 (1979), R. S. Berry, Sci. Am. **263**, 50 (1990).